Supplementary Information (SI) for Journal of Materials Chemistry A.
This journal is © The Royal Society of Chemistry 2025

## Supporting Information

# Tailored Sustainable Synthesis of $Mo_xC$ by Electrochemical Etching of $Mo_2TiAlC_2$ MAX Phase toward Electrochemical Application

**Minhao Sheng [a], Xiaoqing Bin [a], Wenxiu Que [a, *], Yusuke Asakura [b, *],**

**Yusuke Yamauchi [b, c, d*]**

[a] Electronic Materials Research Laboratory, Key Laboratory of the Ministry of Education & International Center for Dielectric Research, Shaanxi Engineering Research Center of Advanced Energy Materials and Devices, School of Electronic Science and Engineering, Xi'an Jiaotong University, Xi'an 710049, P. R. China.

[b] Department of Materials Process Engineering, Graduate School of Engineering, Nagoya University, Nagoya 464-8603, Japan;

[c] Australian Institute for Bioengineering and Nanotechnology (AIBN), The University of Queensland, Brisbane, Queensland 4072, Australia

[d] Department of Chemical and Biomolecular Engineering, Yonsei University, Seoul 03722, South Korea.

## Experimental details

*Materials:* Molybdenum powder (Mo, 2 μm mesh particle size, 99.99%), titanium powders (Ti, 300 mesh, 99.99%), titanium carbide (TiC, 2-4 μm particle size, 99%), aluminum (Al, 400 mesh, 99.9%), graphite powder (C, 99.95%), and potassium sulfide ($K_2S$, 99%) were purchased from Aladdin. Ethyl alcohol ($C_2H_5OH$, 99.5%) was purchased from Sinopharm Chemical Reagent Co., Ltd., China. All chemical reagents were directly used as purchased without further purification.

*Synthesis of $Mo_2TiAlC_2$ powders:* The molar ratio of Mo/Ti/Al/C was 2:1:1.2:1 for the $Mo_2TiAlC_2$ preparation. The powders were mixed with ethyl alcohol in an agate mortar and then dried in an oven at 60°C for 24 h. Subsequently, the powder mixtures were annealed in an atmosphere furnace at 1600°C and held for 4 h under flowing argon gas. After being cooled, the sintered bulk was grinded and sieved through a 400-mesh sieve, thus the powders with a particle size < 38 μm were obtained.

*Purification of Carbon Cloths:* Carbon cloths purification was followed by acetone, ethanol, ultrapure water ultrasonic 20 min, and dried in an oven at 60°C.

*Preparation of $Mo_2TiAlC_2$ anode ceramic disc:* 500 mg of the sifted $Mo_2TiAlC_2$ powders (particle size < 38 μm) were weighed and packed into a 1.2 cm diameter circular die by pressing. The pressure of the tablet press was set to 20 MPa, and the pressure retention time was about 2 min.

*Synthesis of $Mo_xC$@CC:* The electrochemical etching and deposition of MXene are carried out in a two-electrode system. The prepared $Mo_2TiAlC_2$ disc was directly clipped to the electrode holder as the anode. In the electrolytic cell system, carbon cloth (1cm*1cm) was used as the cathode (counter electrode), and the electrolyte consisted 20 mL of 0.05 g mL$^{-1}$ $K_2S$ solution. During the etching process, half of the $Mo_2TiAlC_2$ anode was immersed in the electrolyte with continuous stirring at room temperature. A constant voltage was applied using by a CHI660E electrochemical workstation (Shanghai Chenhua, China) for a duration ranging from several ten minutes to an hour, resulting in the direct deposition on the carbon cloth. The electrocatalyst loadings of $Mo_xC$@CC were obtained by the quantitative difference of carbon cloth before and after etching. The mass loading was regulated by adjusting the duration of the applied voltage. Specifically, under different etching voltage, the etching times for three different mass loadings are approximately as follows: 10 min, 20 min, and 25 min at 3 V; 5 min, 12 min, and 16 min at 4 V; and 2 min, 5 min, and 6 min at 5 V.

*Physical Characterizations:* Micromorphological properties of the samples were observed by a scanning electron microscopy (SEM, JSM6390, JEOL, Japan) and a transmission electron microscopy (TEM, JEM-2010, JEOL, Japan). Microstructural properties of the samples were recorded by an X-ray diffraction diffractometer (XRD, D/max 2200, Rigaku, Japan) using Cu Kα radiation ($\lambda$ = 0.154 nm, 40 kV, 10 mA). Elemental analysis of the samples was fulfilled by an X-ray photoelectron spectroscopy (XPS, ESCALAB 250, VG Thermo, USA) using Al Kα radiation.

*Electrochemical HER Measurements:* The electrochemical HER performances of the prepared electrocatalysts were measured by a three-electrode configuration in 0.5 M $H_2SO_4$ (pH = 0.6) on a CHI660E electrochemical workstation (Shanghai Chenhua, China). Working electrode was CC loaded with above catalytic active materials. Carbon rod electrode was selected as the counter electrode, and SCE as reference electrode in acid electrolyte. According to Nernst equation: E *vs*. RHE (V) = E *vs*. SCE (V) + 0.05916 × pH + 0.244, thus the recorded potential should be corrected by the reversible hydrogen electrode. The linear sweep voltammetry (LSV) and chronoamperometry tests were performed at a scan rate of 5.0 mV $s^{-1}$. The double layer capacitance ($C_{dl}$) of the catalytic active material was recorded by cyclic voltammetry (CV) at various scanning rates (10~100 mV $s^{-1}$) in the non-faradaic potential range. Electrochemical impedance spectroscopy (EIS) was measured using a frequency range from 100 kHz~20 mHz AC voltage with an amplitude of 5 mV. The stability of the electrocatalyst was characterized by a chronoamperometry method with a static current density of 10 mA $cm^{-2}$. During the electrochemical test, nitrogen was continuously injected to eliminate bubbles on the CCs.

*Electrochemical SC Measurements:* The electrochemical tests of the electrode were performed in 0.5 M $H_2SO_4$ aqueous electrolyte using a three-electrode setup in which carbon rod and saturated calomel electrode (SCE) electrodes were served as counter and reference electrodes, respectively. All the electrochemical investigations were carried out on a CHI 660C electrochemical workstation by cyclic voltammetry (CV), galvanostatic charge/discharge. CV tests were carried out from -0.35-0.25 V (vs. SCE). Galvanostatic charge/discharge was performed in the potential range of -0.35-0.25 V (vs. SCE) at different current densities from 1 to 10 A $g^{-1}$. In addition, the long cycle stability test was performed from the LANHE CT2001A tester (LAND, China).

*Preparation of positive electrode (activated carbon)*: Firstly, the pre-mixed slurry was prepared by mixing 95 wt% of the activated carbon (YP-50F) and 5 wt% of polytetrafluoroethylene (PTFE) binder (50 wt% in ethanol). Then, the as-prepared slurry was coated on carbon cloth (Φ 5.4 mm in diameter) to prepare positive electrode. Finally, it was dried in a vacuum oven at 60°C for 12 h.

*Assembly and electrochemical performance test of asymmetric supercapacitors*: The asymmetric supercapacitor (ASC) was assembled using activated carbon (AC) as the positive electrode and $Mo_xC$@CC as the negative electrode, with 0.5 M $H_2SO_4$ aqueous solution serving as the electrolyte and a glass microfiber membrane as the separator. The electrodes were assembled into a two-electrode Swagelok cell configuration. The electrochemical performance of the ASC was evaluated by cyclic voltammetry (CV), galvanostatic charge-discharge (GCD), and long-term cycling stability tests within a voltage window of 0–1 V.

*Preparation of $RuO_2$ electrode*: 5 mg of commercial $RuO_2$ powder was dispersed into a mixed solution containing 475 μL deionized water, 475 μL ethanol, and 50 μL Nafion solution (5 wt%) as a binder. The mixture was ultrasonicated for 30 min to obtain a homogeneous ink. Then, the ink was carefully drop-coated onto a pretreated carbon cloth substrate (1×1 $cm^2$), air-dried at room temperature, and subsequently dried at 60°C in an oven for 12 h to obtain the $RuO_2$@CC electrode.

Computational details: All the calculations were carried out using the Vienna Ab initio Simulation Package (VASP) with the frozen-core all-electron projector-augment wave (PAW) method.[1, 2] The generalized gradient approximation (GGA) proposed by Perdew-Burke-Ernzerhof (PBE) was selected for the exchange-correlation potential.[3] Grimme's method (DFT-D3) was included during the surface adsorption to better evaluate the van der Waals interaction.[4] The cut-off energy for the plane wave was set to 550 eV. The k-space integration was done with Γ-point mesh in the 2D Brillouin zones. The thresholds were $10^{-5}$ eV and 0.03 eV/Å for electronic and ionic relaxations, respectively.

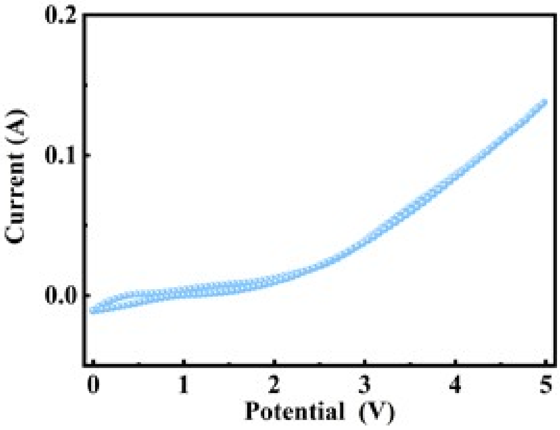

**Figure S1.** CV curves in two electrode system.

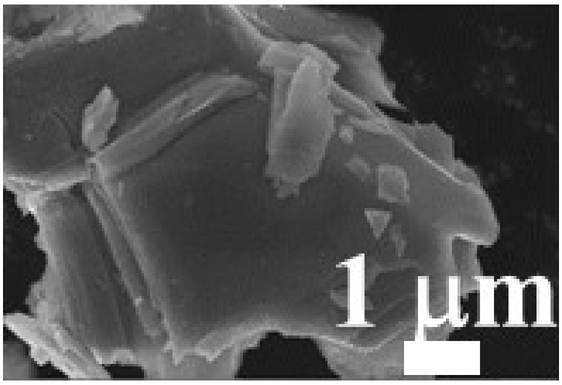

**Figure S2.** SEM image of $Mo_2TiAlC_2$.

**Figure S3.** (a) Picture of the initial solution without anode voltage applied. (b) Picture of the solution with 3 V anode voltage applied for 1 hour. (c) Photo of black material deposited on cathode carbon cloth. (d) The collected solution after several rounds of centrifugation with ultrapure water.

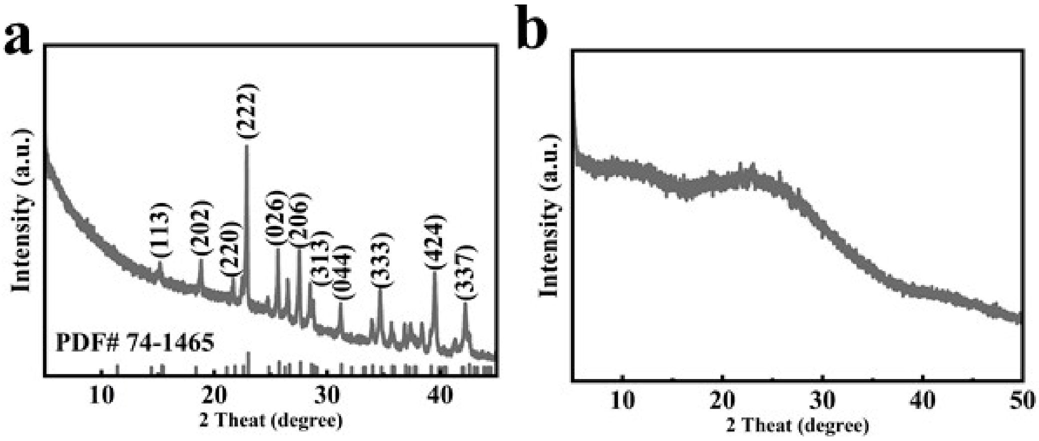

**Figure S4.** (a) XRD of $Mo_xC$ powder in the solution without hot 1 M KOH solution cleaning. (b) XRD of $Mo_xC$ powder in the solution after hot 1 M KOH solution cleaning.

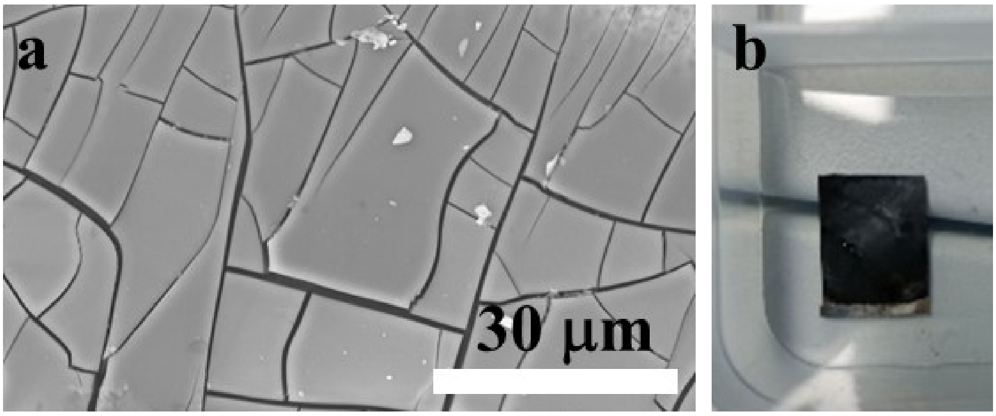

**Figure S5.** (a) SEM image and (b) optical photo of black $Mo_xC$ deposited on the surface of Al foil cathode after electrochemical etching.

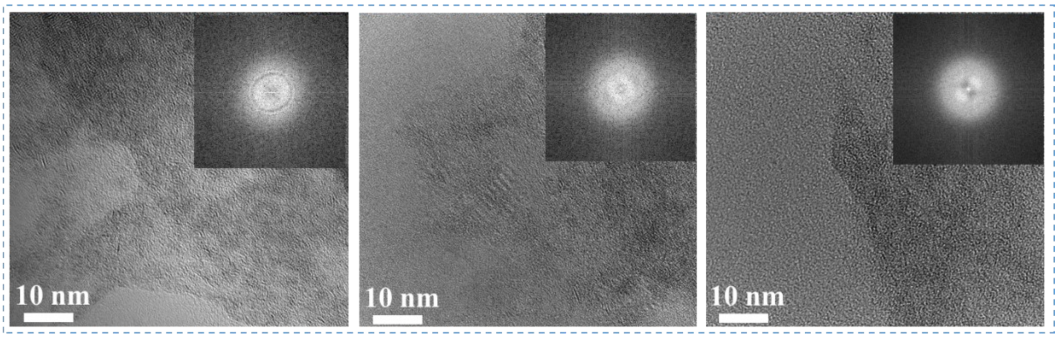

**Figure S6.** HRTEM and the corresponding FFT patterns of $Mo_xC$

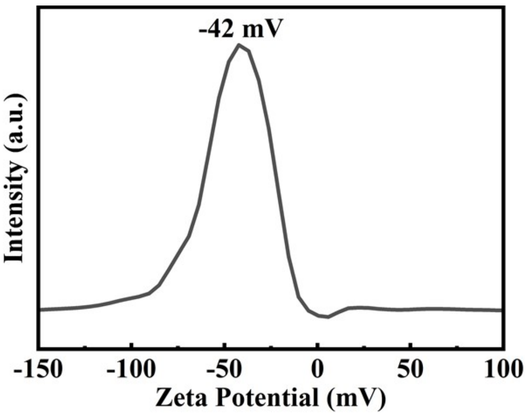

**Figure S7.** Zeta potential of $Mo_xC$

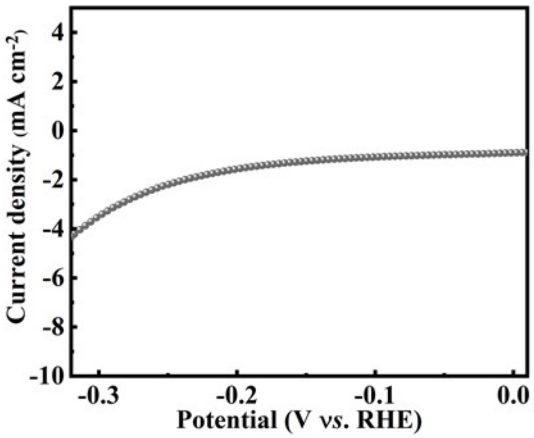

**Figure S8.** LSV of $Mo_2TiAlC_2$ in 0.5 M $H_2SO_4$.

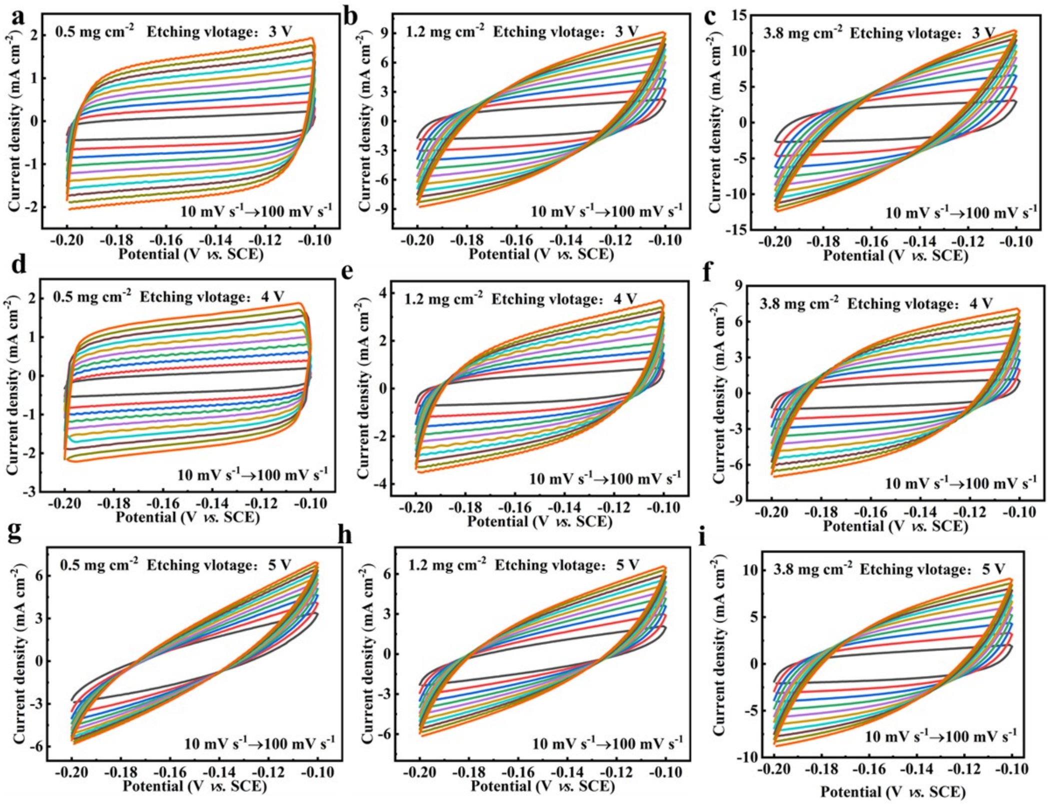

**Figure S9.** $Mo_xC$@CC CV curves of (a) 0.5, (b) 1.2, and (c) 3.8 mg cm$^{-2}$ at 3 V. $Mo_xC$@CC CV curves of (a) 0.5, (b) 1.2, and (c) 3.8 mg cm$^{-2}$ at 4 V. $Mo_xC$@CC CV curves of (g) 0.5, (h) 1.2, and (i) 3.8 mg cm$^{-2}$ at 5 V at various scan rates in 0.5 M $H_2SO_4$.

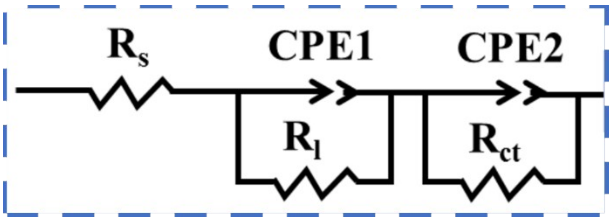

**Figure S10.** Equivalent circuit adopted in the simulation of EIS spectra of Nyquist plot of catalysts.

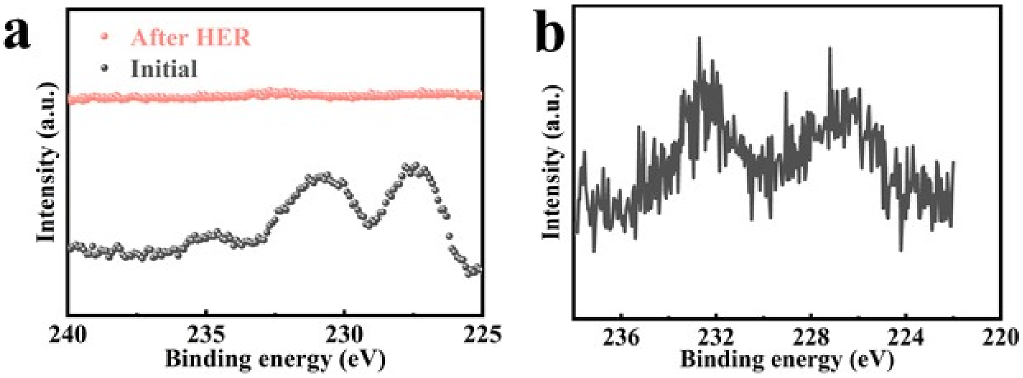

**Figure S11.** (a) XPS spectra of $Mo_xC$@CC before and after HER (-0.3 V vs. RHE) reaction. (b) High-resolution XPS spectra of Mo 3d after HER operation

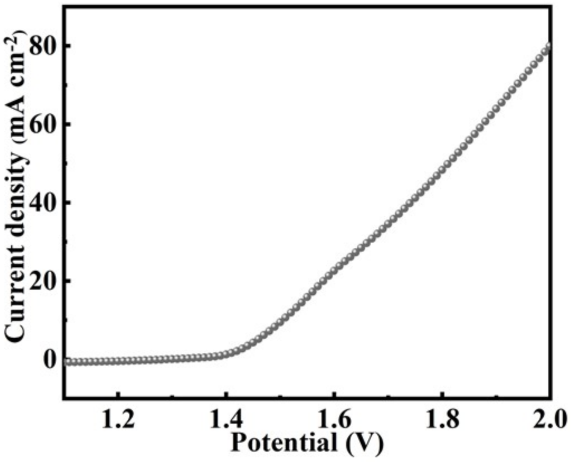

**Figure S12**. LSV curve of overall water splitting based on $Mo_xC$@CC||$RuO_2$@CC.

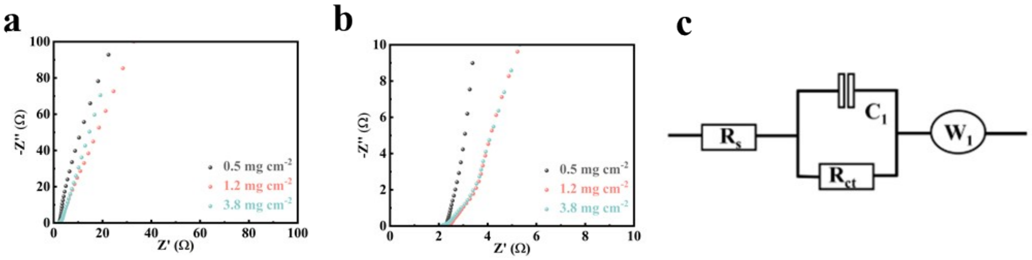

**Figure S13.** (a-b) The electrochemical impedance spectra of the $Mo_xC$@CC (0.2, 1.2, 3.8 mg $cm^{-2}$). (c) The fitting equivalent circuit.

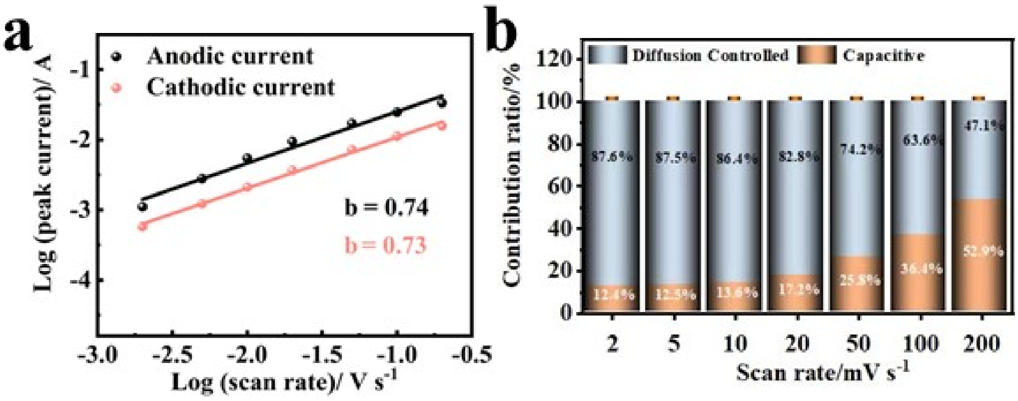

**Figure S14**. The $Mo_xC$@CC electrode: (a) log i versus log v (i is the peak current). (b) Capacitive and diffusion-controlled contribution ratios at different scan rates in CV test.

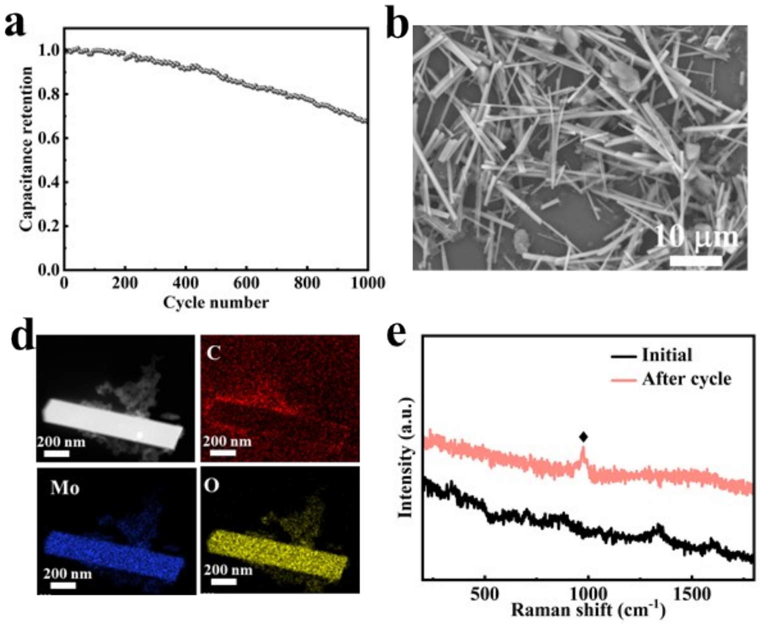

**Figure S15.** (a) Cycling performance curve of symmetry device (1 A g$^{-1}$). (b) SEM image after cycling. (c) TEM image after cycling. (d) Raman spectroscopy after cycling.

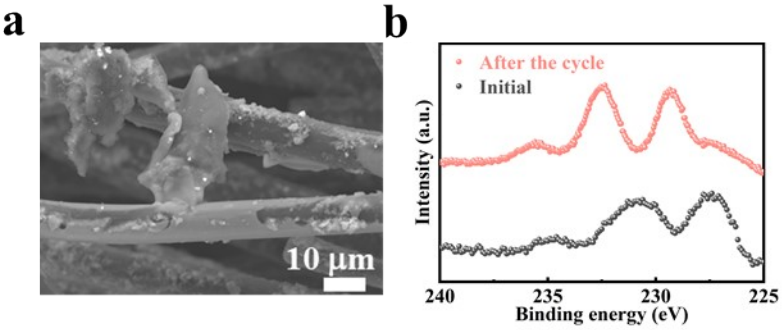

**Figure S16.** Physical characterization of asymmetric devices after cycling (1A g$^{-1}$) (a) SEM image after cycling. (b) XPS after cycling.

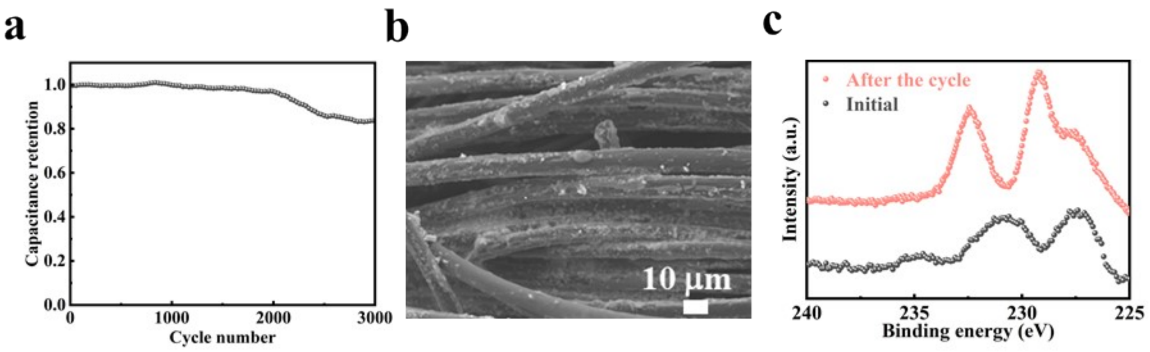

**Figure S17**. (a) Cycling performance curves of asymmetry devices at current density (5 A g$^{-1}$). (b) SEM image after cycling. (c) XPS after cycling.

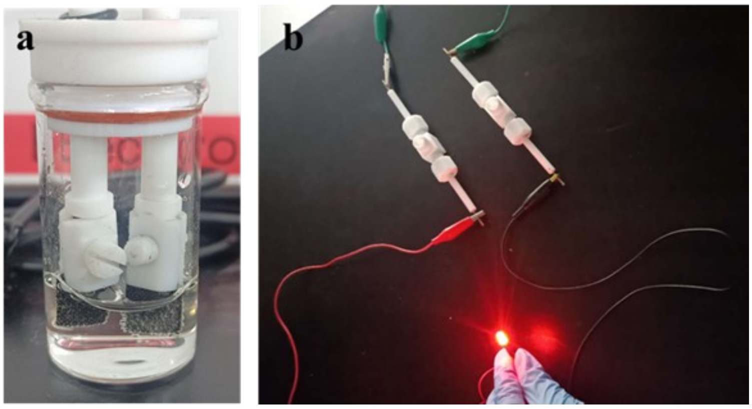

**Figure S18**. Physical demonstration pictures of (a) electrolyzed water and (b) supercapacitor-driven LED lights.

**Table S1.** The change of elemental Mo, Ti, and Al contents of $Mo_xC$@CC before and after electrolysis.

| **Samples** | **Mo (mg/L)** | **Ti (mg/L)** | **Al (mg/L)** |
|---|---|---|---|
| **$Mo_2TiAlC_2$** | 26.740 | 6.93 | 4.78 |
| **$Mo_xC$@CC 3 V** | 24.970 | 0.069 | 0.049 |
| **$Mo_xC$@CC 4 V** | 24.453 | 0.063 | 0.045 |
| **$Mo_xC$@CC 5 V** | 24.123 | 0.052 | 0.038 |

**Table S2.** Synthesis of MXene by traditional acid etching method

| **Catalysts** | **Synthesis time** | **Synthesis temperature** | **Etching solution** |
|---|---|---|---|
| **$Mo_xC$** | 1 h | 20°C | 0.05g/mL $K_2S$<br>(This work) |
| **$Mo_2CT_x$** | 7 d | 55°C | 50%HF[5] |
| **$Mo_2CT_x$** | 7 d | 55°C | 48%HF[6] |
| **$Mo_2CT_x$** | 7 d | 55°C | 50%HF[7] |
| **$Mo_2CT_x$** | 7 d | 55°C | 50%HF[8] |
| **$Mo_2TiC_2T_x$** | 48 h | 55°C | 50%HF[9] |
| **$Mo_2TiC_2T_x$** | 72 h | 55°C | 50%HF[10] |
| **$Mo_2TiC_2T_x$** | 6 d | 20°C | 40%HF[11] |
| **$Mo_2TiC_2T_x$** | 60 h | 55°C | 49%HF[12] |
| **$Mo_2TiC_2T_x$** | 72 h | 55°C | 40%HF[13] |
| **$Mo_2TiC_2T_x$** | 72 h | 55°C | 49%HF[14] |
| **$Mo_2TiC_2T_x$** | 72 h | 55°C | 49%HF[15] |
| **$Mo_2TiC_2T_x$** | 48 h | 55°C | 49%HF[16] |
| **$Mo_2TiC_2T_x$** | 7 d | 60°C | 48-51% HF[17] |
| **$Mo_2Ti_2C_3T_x$** | 90 h | 55°C | 50%HF[9] |
| **$Mo_{1.33}CT_x$** | 24 h | 20°C | 28M HF[18] |
| **$Mo_{1.33}CT_x$** | 120 h | 20°C | 25%HF[19] |

**Table S3.** Fitted parameters of the EIS data of the two catalysts.

| Catalysts | $R_s$ (Ω) | $R_l$ (Ω) | CPE1-T | CPE1-P | $R_{ct}$ (Ω) | CPE2-T | CPE2-P |
|---|---|---|---|---|---|---|---|
| **Mo$_x$C@CC 3 V<br>0.5 mg cm$^{-2}$** | 2.212 | 0.20647 | 0.0047948 | 0.8437 | 51.12 | 0.011327 | 0.92063 |
| **Mo$_x$C@CC 3 V<br>2.0 mg cm$^{-2}$** | 1.959 | 0.37053 | 0.12442 | 0.48583 | 19.65 | 0.20712 | 0.90127 |
| **Mo$_x$C@CC 3V<br>3.8 mg cm$^{-2}$** | 2.326 | 0.16394 | 0.021465 | 0.70756 | 14.66 | 0.10569 | 0.76666 |
| **Mo$_x$C@CC 4 V<br>0.5 mg cm$^{-2}$** | 2.249 | 0.32906 | 0.0010651 | 0.83412 | 77.69 | 0.044135 | 0.71637 |
| **Mo$_x$C@CC 4 V<br>2.0 mg cm$^{-2}$** | 2.190 | 0.13278 | 0.0028132 | 0.89067 | 17.00 | 0.093756 | 0.75295 |
| **Mo$_x$C@CC 4 V<br>3.8 mg cm$^{-2}$** | 2.201 | 0.33997 | 0.22938 | 0.45074 | 7.43 | 0.22938 | 0.45074 |
| **Mo$_x$C@CC 5 V<br>0.5 mg cm$^{-2}$** | 2.314 | 0.18487 | 0.0011489 | 0.94169 | 11.41 | 0.087413 | 0.79333 |
| **Mo$_x$C@CC 5 V<br>2.0 mg cm$^{-2}$** | 2.546 | 1.395 | 0.010719 | 0.61504 | 8.43 | 0.048758 | 0.73717 |
| **Mo$_x$C@CC 5 V<br>3.8 mg cm$^{-2}$** | 2.354 | 1.338 | 0.051605 | 0.45266 | 12.43 | 0.08047 | 0.70677 |

**Table S4.** Supercapacitor Device Performance Comparison.

| **Electrodes** | **Electrolyte** | **Energy Density** | **Cycle stability** | **Ref.** |
|---|---|---|---|---|
| $Mo_xC$@CC//AC | 0.5 M $H_2SO_4$ | 12.4 W h $kg^{-1}$ | 80.2% after 6000 cycles (1 A $g^{-1}$) | This work |
| **$RuO_2$–$MoO_3$/Ti// $IrO_2$–ZnO/Ti** | 0.5 M $H_2SO_4$ | 10.9 W h $kg^{-1}$ | 91.3% after 5000 cycles (1 A $g^{-1}$) | 20 |
| **d-$V_4C_3T_x$//d-$V_4C_3T_x$** | 1.0 M $H_2SO_4$ | 4.1 Wh $kg^{-1}$ | 99.0% after 10,000 cycles (10 A $g^{-1}$) | 17 |
| **HPC//HPC** | 1.0 M $H_2SO_4$ | 9 Wh $kg^{-1}$ | 70% after 1000 cycles | 21 |
| **PNAS/CC//PNAS/CC** | PVA/$H_2SO_4$ | 1.1 Wh $kg^{-1}$ | 88% after 10,000 cycles （5 A $g^{-1}$） | 22 |
| **NHPC-0.5//NHPC-0.5** | 1.0 M $H_2SO_4$ | 11.3 Wh $kg^{-1}$ | 99% after 12,000 cycles （6.7 A $g^{-1}$） | 23 |
| **PANI-Ni//PANI-Ni** | 1.0 M $H_2SO_4$ | 31.5 Wh $kg^{-1}$ | 83% after 1000 cycles （5 A $g^{-1}$） | 24 |

1 G. Kresse and D. Joubert, *Phys. Rev. B*, 1999, **59**, 1758-1775.

2 G. Kresse and J. Furthmüller, *Phys. Rev. B*, 1996, **54**, 11169-11186.

3 K. B. John P. Perdew, Matthias Ernzerhof, *Phys. Rev. Lett.*, 1996, **77**, 3865-3868.

4 S. Grimme, J. Antony, S. Ehrlich and H. Krieg, *J. Chem. Phys.*, 2010, **132**, 154104.

5 Z. W. Seh, K. D. Fredrickson, B. Anasori, J. Kibsgaard, A. L. Strickler, M. R. Lukatskaya, Y. Gogotsi, T. F. Jaramillo and A. Vojvodic, *ACS Energy Lett.*, 2016, **1**, 589-594.

6 K. R. G. Lim, A. D. Handoko, L. R. Johnson, X. Meng, M. Lin, G. S. Subramanian, B. Anasori, Y. Gogotsi, A. Vojvodic and Z. W. Seh, *ACS Nano*, 2020, **14**, 16140-16155.

7 M. Yi, S. Hu, N. Li, H. Wang and J. Zhang, *J. Energy Chem.*, 2022, **72**, 453-464.

8 J. Liang, C. Ding, J. Liu, T. Chen, W. Peng, Y. Li, F. Zhang and X. Fan, *Nanoscale*, 2019, **11**, 10992-11000.

9 A. D. Handoko, K. D. Fredrickson, B. Anasori, K. W. Convey, L. R. Johnson, Y. Gogotsi, A. Vojvodic and Z. W. Seh, *ACS Appl. Energy Mater.*, 2017, **1**, 173-180.

10 W. Ren, Z. Chang, J. Zhang, L. Wang and C. Xu, *ACS Appl. Energy Mater.*, 2022, **5**, 15828-15833.

11 J. Luxa, P. Kupka, F. Lipilin, J. Sturala, A. Subramani, P. Lazar and Z. Sofer, *ACS Catal.*, 2024, **14**, 15336-15347.

12 Z. Wu, J. Shen, C. Li, C. Zhang, K. Feng, Z. Wang, X. Wang, D. M. Meira, M. Cai, D. Zhang, S. Wang, M. Chu, J. Chen, Y. Xi, L. Zhang, T. K. Sham, A. Genest, G. Rupprechter, X. Zhang and L. He, *ACS Nano*, 2022, **17**, 1550-1559.

13 G. Li, B. Zhou, P. Wang, M. He, Z. Fang, X. Yuan, W. Wang, X. Sun and Z. Li, *Catalysts*, 2022, **12**, 850.

14 L.-H. Zheng, C.-K. Tang, Q.-F. Lü and J. Wu, *Int. J. Hydrogen Energy*, 2022, **47**, 11739-11749.

15 J. Wang, P. He, Y. Shen, L. Dai, Z. Li, Y. Wu and C. An, *Nano Res.*, 2021, **14**, 3474-3481.

16 J. Zhao, W. Yan, Z. Liu, X. Liu, Y. Tian and X. Cui, *Nano Res.*, 2024, **17**, 7174–7181.

17 X. Bin, M. Sheng, B. Kong, Y. Luo, J. Xiao and W. Que, *Nanoscale*, 2024, **16**, 15196-15207.

18 S. Intikhab, V. Natu, J. Li, Y. Li, Q. Tao, J. Rosen, M. W. Barsoum and J. Snyder, *J. Catal.*, 2019, **371**, 325-332.

19 A. S. Etman, J. Halim and J. Rosen, *Nano Energy*, 2021, **88**, 106271.

20 K. Feng, Z. Ye, J. Guo, Y. Lin, Y. Zhang, Q. Ma, Y. Shao and K. Chen, *J. Alloys Compd.*, 2020, **819**, 153385.

21 X. Wu, X. Yang, W. Feng, X. Wang, Z. Miao, P. Zhou, J. Zhao, J. Zhou and S. Zhuo, *Nanomaterials*, 2021, **11**, 2838.

22 Y. Tian, Y. Yang, Y. Wu, Z. Zhou, Y. Li, J. Wang, S. Liu and C. Wang, *J. Energy Storage*, 2023, **72**, 108308.

23 H. Sun, H. Quan, M. Pan, Z. Zhang, Y. Zeng and D. Chen, *J. Alloys Compd.*, 2020, **826**, 154208.

24 Y. Xie and X. Sha, *Synthetic Metals*, 2018, **237**, 29-39.